Infrared-absorption spectrum of the electron bubble in liquid helium

C. C. Grimes and G. Adams
AT&T Bell Laboratories, Murray Hill, New Jersey 07974
(Received 29 July 1991)

The energy of the electronic transition from the ground state to the first excited state in the electron bubble in liquid helium has been measured by direct infrared absorption at pressures from zero to the solidification pressure and at temperatures from 1.3 to 4.2 K. At 1.3 K the $1s$-$1p$ splitting varies from 0.102 eV at $P=0$ to 0.227 eV at $P=25$ atm. At intermediate pressures a simple spherical-square-well model calculation fits the measured splittings within a few percent if the surface tension is taken to be independent of pressure. This model, when extended to allow for dilation and elongation of bubbles trapped on vorticity and dilation of rapidly drifting bubbles, agrees well with the observed transition energies at all pressures. The measured linewidths are larger by at least a factor of 2 than those calculated, which may indicate heating of rapidly drifting bubbles.

INTRODUCTION

An excess electron in liquid helium resides in a cavity or bubble of radius ≈ 17 Å at zero pressure.[1] The electron-bubble state occurs because the Pauli-principle repulsion between an electron and helium atoms is strong, while the attractive polarization interaction is weak. The electron bubble that results is nearly a textbook example of an electron confined in a spherical-square-well potential about 1 eV deep.

Northby and Sanders performed the first spectroscopic study on the electron bubble when they observed electronic transitions from the ground state to the continuum at a wavelength near 1.0 μm.[2] Their photoconductivity measurement was extended by Zipfel and Sanders to finite pressures and longer wavelengths (2.5 μm) where transitions to a bound state were observed.[3,4] Following the suggestion of Miyakawa and Dexter[5] (MD), Grimes and Adams[6] (GA) recently observed the $1s$-$1p$ transition at still longer wavelengths (≈ 11 μm at 1 atm pressure). All of these spectroscopic studies employed a not-well-understood photoconductive mechanism to detect the transitions. The photoconductive effect (an increase in electron-bubble drift current when resonant radiation is incident on the bubbles) operates only over a relatively small region of the P-T plane, and appears to be associated with trapping of bubbles on vorticity in the superfluid helium.[6]

To study the spectra of electron bubbles over all of the accessible portion of the P-T plane, we have modified the apparatus used earlier and have observed the $1s$-$1p$ transition in direct infrared absorption. In absorption, we have measured the energy of the $1s$-$1p$ transition and its variation with pressure from $P=0$ to the solidification pressure at 1.3 K. We have also measured the variation of the transition energy with temperature from 1.2 to 4.2 K at 2.9 atm. This contrasts with the earlier photocurrent study where the signal vanished at both low and high pressures and at temperatures above 1.6 K.[6] Very recently, Parshin and Pereverzev reported observing the $1s$-$1p$ transition by direct absorption at a single wavelength.[7] Our measured transition energies are compared with calculations based on the spherical-square-well (SSW) model and its extension to elongated bubbles trapped on vorticity. This comparison yields some evidence that at low pressures bubbles trapped on vorticity are slightly dilated and elongated.

APPARATUS AND PROCEDURES

To observe the $1s$-$1p$ transition in absorption, we have employed a cell that is relatively long and thin compared to cells used in the earlier photoconductivity measurements. The absorption cell, shown schematically in Fig. 1, contains eight field-emission tips which serve as sources of electrons. The increased cell length (5.4 cm) provides a longer optical path and the small i.d. (0.63 cm) insures that the infrared radiation passes near the field-emission tips where the electron density is greatest. A mercury-cadmium-telluride infrared detector is mounted on the bottom of the cell and is coupled to it through a small aperture. The infrared radiation, as described previously, originates in a Nernst glower, passes through a chopper and a monochromator, and is guided to the cell by a polished brass light pipe and concentrator cone.[6] The walls of the cell were carefully polished and gold plated for high reflectivity. We estimate that the infrared radiation makes about ten transits through the cell. The cell is immersed in a pumped helium bath and is filled with liquid helium which can be pressurized to 35 atm.

The infrared radiation entering the cell is chopped at 1 kHz and the field-emission current is modulated at about 10 Hz. The infrared wavelength is swept while the output of the infrared detector is rectified in two lock-in detectors operating in series. The first lock-in operates at 1 kHz and derives its reference from the chopper, so its output is proportional to the photon flux incident on the detector. The second lock-in operates at 10 Hz and is phase-locked to the ac voltage that modulates the field-emission current, so its output is proportional to the in-

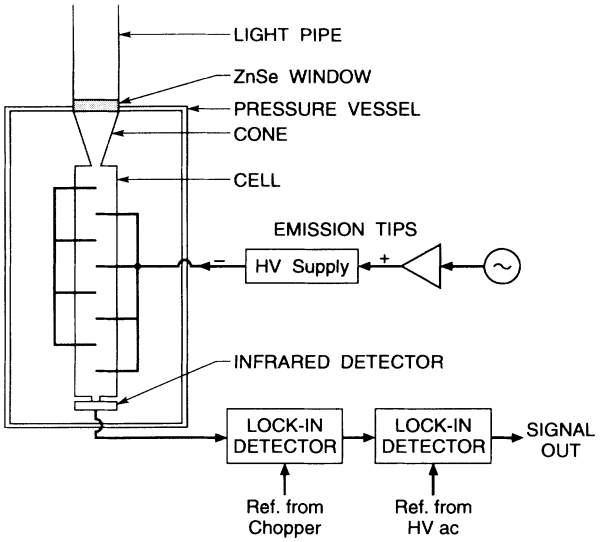

FIG. 1. Schematic diagram of the infrared absorption cell and the instruments used to observe electronic transitions in electron bubbles. Eight field-emission tips in parallel provide a 1-μA source of electrons. Chopped infrared radiation in the 4–14 μm region is detected by a Hg-Cd-Te infrared detector.

frared attenuation caused by the electrons. The output of this lock-in is recorded versus wavelength. In our experimental traces we plot increasing absorption upwards. Examples of experimental traces taken at three different pressures are shown in Fig. 2.

The absorption data traces are first normalized to the photon flux into the cell, and then a Gaussian line shape is fitted to the data. Next, the position of the line center obtained from the fit is corrected for the lag due to the response time of the system and for the lash in the gear system that rotates the diffraction grating. The transition energies obtained from the line centers are then plotted versus the pressure in the cell.

EXPERIMENTAL RESULTS AND DISCUSSION

Figure 3 displays the transition energies at low T obtained both from absorption measurements and the earlier photocurrent measurements. Note that the absorption measurements span all pressures up to the solidification pressure.

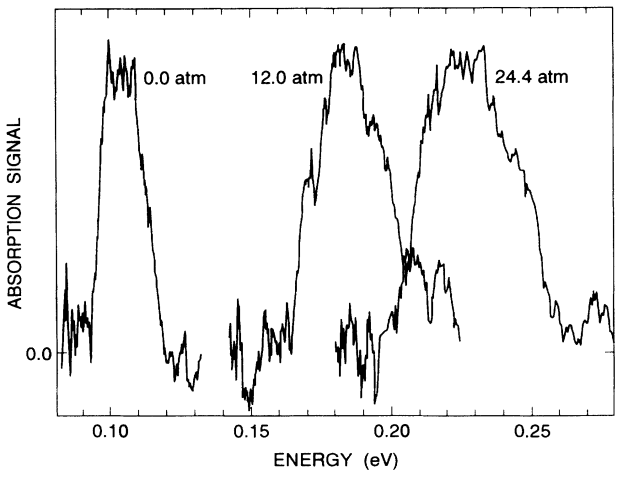

FIG. 2. Representative absorption signals for 1s-1p transitions in the electron bubble at three different pressures.

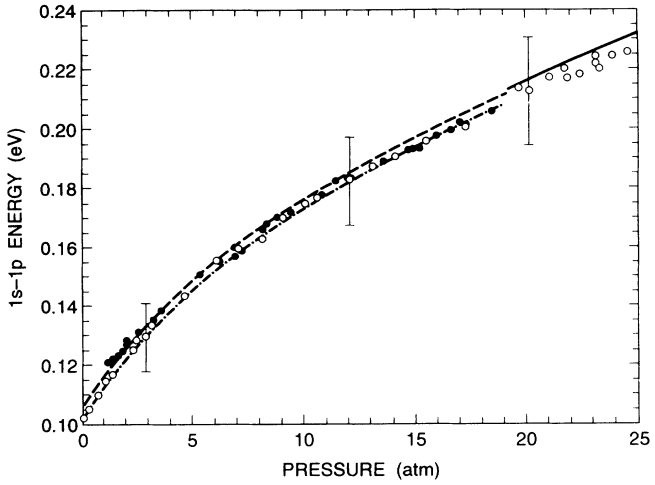

FIG. 3. Energy of the 1s-1p transition in electron bubbles at ≈ 1.3 K plotted vs pressure. The open circles are from direct infrared-absorption measurements and the filled circles are from earlier photocurrent measurements. Absorption linewidths are indicated by the vertical bars on three of the points. The continuous curve displays the calculated transition energies for free electron bubbles. The dashed curves display the calculated splitting of the m manifold of the final state due to elongation of bubbles trapped on vorticity. The observed transitions are too broad to resolve such a splitting.

The photocurrent data points displayed in Fig. 3 extend only from $P=1$ atm to $P=18$ atm. The photocurrent detection mechanism simply did not work outside this region. GA showed that the photocurrent vanished along a line in the P-T plane[8] where electron bubbles are no longer trapped on vorticity. This indicates that the photocurrent mechanism involves trapping of bubbles on vorticity, and several such mechanisms have been proposed and were described in GA. However, the details of the detection mechanism are not fully understood.

Spherical-square-well model

In the simple SSW model the electron is viewed as residing in a finite-depth spherical-square-well potential. The bubble radius is determined by the equilibrium between the inward pressures due to surface tension, pressure, and polarization in the liquid and the outward pressure due to localization of the electron. The total energy of the electron becomes

$$E_T = E_e + \tfrac{4}{3}\pi R^3 P + 4\pi R^2 \sigma - (\epsilon - 1)e^2/2\epsilon R \ , \qquad (1)$$

where E_e is the ground-state electronic energy, the second term is the pressure-volume work done in forming the cavity, the third term is the surface energy, and the last term is the polarization energy. The electronic eigenenergies for finite SSW potentials of depth V_0 are treated in textbooks.[9] The eigenenergies take the form $E_{nl} = C_{nl}(V_0)/R^2$, where the $C_{nl}(V_0)$ are obtained from simple transcendental equations. Using the experimen-

tally known quantities $\sigma=0.341$ erg/cm^2,[10] $\epsilon=1.057$,[11] $V_0(0)=1.02$ eV,[12] and minimizing the total energy yields the $P=0$ equilibrium radius of 17.2 Å. For a bubble of this radius, the surface tension exerts a pressure on the electron equivalent to $P\approx 4$ atm.

Earlier articles on the calculated spectral properties of the electron bubble were reviewed in Ref. 1 and were described in GA. MD (Ref. 5) used the SSW model to treat in detail the two allowed electric-dipole absorption transitions: $1s$-$1p$ and $1s$-$2p$. They calculated the transition energies and absorption cross sections as a function of pressure. Note that each term in Eq. (1) depends upon the external pressure. The electronic term depends upon V_0, which varies with the liquid density, the pressure appears explicitly in the second term, and in the last two terms σ and ϵ vary with the liquid density. MD found that $V_0(P)$ increased about 20% over the pressure interval 0–25 atm for both an optical approximation and a Wigner-Seitz (WS) model calculation. They incorporated the WS pressure variation of $V_0(P)$ in their calculations and we have used it in our calculations. MD assumed that $\sigma(P)$ varied with P according to the theory of Amit and Gross.[13] Consequently, they took σ to vary from 0.36 at $P=0$ to 0.66 erg/cm^2 at $P=25$ atm. However, GA found that their photocurrent data on the $1s$-$1p$ transition energy and Zipfel's data on the $1s$-$2p$ transition[4] could simultaneously be fitted using the SSW model if the surface tension were taken to be 0.341 erg/cm^2 independent of P. The resulting pressure dependence of the $1s$-$1p$ transition energy is displayed as the continuous line in Fig. 3.

The SSW model also yields the electron-bubble radius $R(P)$ as a function of P. The SSW radii corresponding to the line shown in Fig. 3 were displayed by GA and compared with other $R(P)$ determinations. The bubble radius obtained from the SSW model varies from 17.2 to 11.1 Å as P increases from 0 to 25 atm.

The simple SSW model, with no adjustable parameters except our setting $\sigma(P)$ equal to the $P=0$ measured value, comes very close to fitting both our data and Zipfel's photoconductivity data on the $1s$-$2p$ transition. However, there are additional corrections which should be made to the SSW model, and these are described below.

Distorted bubble model

In the region of the P-T plane where photocurrent data were obtained (roughly $P<18$ atm and $T<1.6$ K), electron bubbles injected from field-emission tips spend a large fraction of their transit time through the cell trapped on vorticity. At T's and P's above this region the electron bubbles are untrapped.

In the following we show that the anisotropic Bernoulli pressure acting on an electron bubble trapped on a vortex line slightly expands and elongates the bubble and this decreases the $1s$-$1p$ splitting. We assume a bubble shape of the form

$$R=R_0[1+(\beta/2)(3\cos^2\theta-1)]\ ,$$

and for the ground-state energy of the bubble we use

$$E=E_0+E_v+E_s+E_{\rm sub}\ ,$$

where

$$E_0=E_e(1+0.52\beta^2)\ ,\quad E_v=\tfrac{4}{3}\pi R_0^3 P(1+\tfrac{3}{5}\beta^2)\ ,$$

$$E_s=4\pi R_0^2\sigma(1+\tfrac{4}{5}\beta^2)\ ,$$

$$E_{\rm sub}=-(2\pi\rho_s\hbar^2 R_0/M_{\rm He}^2)\times[(1+a^2/R_0^2)^{1/2}\sinh^{-1}(R/a)-1](1+\beta)\ .$$

Here the electronic energy E_e is the finite-well value with the elongation factor from Gross and Tung-Li,[14] the volume and surface terms use expressions from Lord Rayleigh,[15] and the substitution energy $E_{\rm sub}$ is obtained from that of Donnelly and Roberts.[16] The substitution energy is approximately the kinetic energy of the circulating superfluid displaced by the bubble. This expression was derived by Donnelly and Roberts assuming that the superfluid density vanishes at the vortex core according to an expression given by Fetter which contains a healing length, a.[17] We take $a=1.46$ Å as suggested by Parks and Donnelly.[18] Since the superfluid velocity about the vortex varies as $1/r$, the substitution energy favors elongation of the bubble along the vortex axis. That is, the Bernoulli effect causes the pressure on a trapped bubble to be greatest at its equator and least near its poles, and this variation elongates the bubble.

Using the expressions above and taking the well depth to be 1.02 eV and $\sigma=0.341$ erg/cm^2, we find at $P=0$ and for $\beta=0$, the equilibrium radius of a spherical bubble centered on a vortex line is expanded by 1.4% to 17.4 Å. This expansion alone lowers the calculated transition energy from 0.1061 eV for a free bubble to 0.1036 eV for a trapped bubble. This is close to the observed value of 0.1028 eV.

Now, minimizing the total energy at $P=0$, we find $\beta=0.023$ or an elongation of 2.3%. Although this distortion of the bubble lowers the total energy, it changes the electronic energy of the ground state less than 1 meV.

Since the size and shape of the bubble do not relax during an optical transition, the elongation of the bubble removes the degeneracy of the m manifold for the excited p states. The $m=0$ p state is lowered in energy while the $m=\pm 1$ p states are raised in energy relative to the spherical bubble. The change in the electronic energy of p states due to such a quadrupolar deformation has been treated by DuVall and Celli.[19] They present plots of the p-state electronic energies versus β for a variational calculation and a perturbation calculation for both an infinite well and a 1-eV-deep well. Using the initial slopes of their plots for the 1-eV well, we find for $\beta=0.023$ that the energy of the $m=0$ state is lowered 1.24% and that of the $m=\pm 1$ states is raised by 0.66%. The corresponding $1s$-$1p$ transition energies at $P=0$ are then 0.1011 eV and 0.1049 eV, respectively. The calculated variations of these transition energies with pressure are displayed in Fig. 3 as the dashed lines. We do not expect to observe this splitting of the m manifold, because it is small compared to the observed linewidths.

Drifting bubbles

At high T and P the bubbles spend a negligible fraction of the transit time trapped on vortices. Consequently, their drift velocities increase until they are limited by mobility and space-charge effects. Below we estimate that the drift velocity is ≈ 1000 cm/sec. The Bernoulli pressure at the waist of the drifting bubble is then comparable to that when it is centered on a vortex line, so the expansion is comparable. However, the anisotropy is opposite: the drifting bubble should be an oblate spheroid instead of the prolate spheroid on a vortex line. In an oblate spheroid the degeneracy of the m manifold of the p states is again removed, but in the opposite sense than for the prolate spheroid. The corresponding splittings of the $1s$-$1p$ transition are again small relative to the observed linewidth. If the measurements were performed at sufficiently low temperatures, these interesting effects might be resolved.

Linewidth

The linewidth measured at 1.3 K increases monotonically with pressure from ≈ 0.018 eV at 0 atm to ≈ 0.039 eV at 25 atm. Although there is appreciable scatter in the linewidth data, the full width at half maximum is very nearly one-sixth of the transition energy at all pressures.

The contributions of the thermally excited vibrational modes of the bubble to the linewidth of the $1s$-$1p$ transition at $P=0$ have been estimated by Fowler and Dexter[20] (FD) using classical configuration coordinate theory.[21] They found at 1.3 K the $l=0$ (breathing) mode contributes ≈ 0.0025 eV and the $l=2$ (quadrupole) mode contributes ≈ 0.010 eV to the linewidth of the transition. We have repeated these calculations using the bubble parameters obtained from fitting the spectroscopic data to the SSW model and using the results of DuVall and Celli described above. We find at $P=0$ and $T=1.3$ K, the $l=0$ mode contributes ≈ 0.006 eV and the $l=2$ modes contribute ≈ 0.0055 eV to the linewidth. Convolution of these two contributions yields ≈ 0.0081 eV for the linewidth.

For bubbles trapped on vorticity, there is an additional contribution to the linewidth due to the static elongation of the bubble which splits the m manifold of the p state by 0.0038 eV as described above. Including this effect increases the linewidth to ≈ 0.009 eV and introduces an asymmetry in the line shape which causes it to rise more steeply on the short-wavelength side. Since the measured linewidth at 1.3 K and $P=0$ is ≈ 0.018 eV, it is about twice the calculated linewidth.

The observed linewidth may be broadened due to heating of the vibrational modes of the bubble above the bath temperature. To obtain bubble densities large enough to study the $1s$-$1p$ transition, we typically apply -2500 V to the field-emission tips. This produces space-charge limited currents of $\approx 10^{-7}$ A per tip. We estimate that bubbles not trapped on vorticity have drift velocities of ≈ 1000 cm/s, which is approximately twice the bubble's thermal velocity at 1.3 K. Consequently, we expect the internal degrees of freedom of such bubbles to be out of thermal equilibrium with the bath. However, decreasing the field-emission current by a factor of 4 did not appear to reduce the linewidth, but it did seriously lower the signal-to-noise ratio.

As mentioned earlier, Parshin and Pereverzev have recently reported observing the $1s$-$1p$ transition by direct absorption.[7] Their data were taken at a fixed wavelength of 6.7 μm while sweeping P at fixed Ts of 2.2, 3.0, and 4.2 K. Their transition positions and linewidths are consistent with ours. As an electron source they used a β emitter with a saturation current density of 1.5×10^{-8} A/cm^2. To enhance the average electron-bubble density they applied an rf electric field of 10^4 V/cm. Such a strong electric field may have heated the bubbles above the bath temperature.

Line shape

Although the line shape is expected to be approximately a Gaussian and we have fitted a single Gaussian to each of our experimental lines to determine the positions of the line centers, the observed lines frequently have relatively flat tops and steep sides. Such lines look like a superposition of two or more Gaussians. The lines shown in Fig. 2 are not as sharply peaked as Gaussians should be, and a fit to each of a single Gaussian is not quite as good as a fit to a sum of two Gaussians. As described above, for prolate bubbles trapped on vorticity we expect the line shape to be a superposition of two unresolved lines with the higher-energy line having twice the intensity of the lower one. For rapidly drifting oblate bubbles we expect the lower-energy line to be the more intense. To search for such effects, we have fitted pairs of Gaussians to many of our data traces and the expected trend appears to exist. That is, the stronger component of the pair of lines has the higher energy at low T and P and shifts to have the lower energy when T and P are above the vortex trapping region. However, our signal-to-noise ratio was marginal for this kind of study. If the experiment were performed at lower temperatures in an apparatus having a longer cell and using more nearly optimized detectors and gratings, these interesting effects might be more clearly resolved.

Variation with temperature

Figure 4 displays the variation of the $1s$-$1p$ transition energy with T at $P=2.9$ atm. The decrease in transition energy with increasing T simply reflects the increase of the bubble radius due primarily to the decrease in surface tension. At a free surface where $P(T)$ equals the saturated vapor pressure, $\sigma(T)$ decreases by nearly a factor of 4 between 1.3 and 4.2K.[10] Incorporating the density dependence of ϵ and V_0 and taking the T dependence of σ at 2.9 atm to be similar to that at saturated vapor pressure the SSW model yields the continuous line in the figure. The bubble radius calculated using the SSW model expands by 14% between 1.3 and 4.2 K.

The measured linewidth increases by a factor of approximately 1.8 between 1.3 and 4.2 K. Since there are contributions to the linewidth that are not yet under-

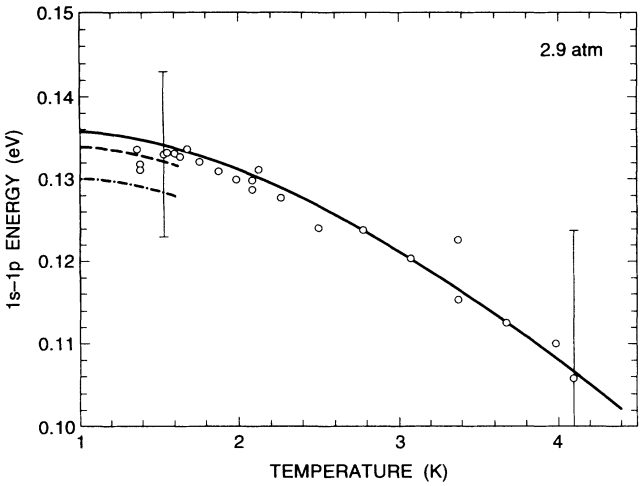

FIG. 4. Energy of the $1s$-$1p$ transition displayed vs temperature at a constant pressure of 2.9 atm. The vertical bars on some points indicate the linewidths. The continuous line is obtained from a spherical-square-well model for free bubbles. The dashed curves are calculated for elongated bubbles trapped on vorticity.

stood, application of configuration coordinate theory to deduce a bubble normal-mode frequency from the T dependence of the linewidth yields only approximate results. Using the standard single-mode approximation, the factor of 1.8 increase yields a normal-mode frequency of ≈ 25 GHz.[21] This agrees qualitatively with the calculated frequencies of 15 GHz for the breathing mode and 30 GHz for the quadrupole mode at 2.9 atm and 1.3 K.[22]

OTHER SYSTEMS

Now that we have shown that it is feasible to study the absorption spectra of electron bubbles in normal liquid helium, the same experimental techniques should be applicable to the other liquids where electrons create bubbles. The other liquids are expected to be ^{3}He, hydrogen, deuterium, and neon. For liquid hydrogen one can combine the measured barrier height[23] with Miyakawa and Dexter's calculated transition energies[24] to deduce that the $1s$-$1p$ absorption should occur at wavelengths between 4 and 7 μm for T between 20 and 34 K. There is evidence that electron bubbles also exist in the solid forms of these materials.[25] However, the bubble mobilities are many orders of magnitude smaller in the solids than in the liquids, so it would be very difficult to modulate the density of electron bubbles at a rate high enough to use lock-in detection techniques.

CONCLUSIONS

The $1s$-$1p$ transition in the electron bubble in liquid ^{4}He has been studied by direct infrared absorption from $P=0$ to the solidification pressure and from 1.3 to 4.2 K. At intermediate pressures, the transition energies agree with earlier photocurrent data and are described within a few percent by a simple spherical-square-well model provided the surface tension is taken to be independent of pressure. This model, when modified to allow for dilation and elongation of bubbles trapped on vorticity and dilation of rapidly drifting bubbles, agrees well with the observed transition energies. The observed linewidths are larger by at least a factor of 2 than those calculated from the model. In some regions of temperature and pressure, heating of rapidly drifting bubbles may be contributing to the linewidth.

ACKNOWLEDGMENTS

We gratefully acknowledge the advice provided by D. H. Rapkine and G. A. Thomas and their loans of equipment. We have benefited from numerous discussions with Veit Elser.

[1]For comprehensive reviews of electrons in helium, see A. L. Fetter, in *The Physics of Liquid and Solid Helium* edited by K. H. Bennemann and J. B. Ketterson (Wiley, New York, 1974), Pt. I, Chap. 3; K. W. Schwarz, in *Advances in Chemical Physics XXXIII,* edited by L. Prigogine and S. A. Rice (Wiley, New York, 1975), p. 1; and V. B. Shikin, Usp. Fiz. Nauk **121**, 457 (1977) [Sov. Phys. Usp. **20**, 226 (1977)].

[2]J. A. Northby and T. M. Sanders, Phys. Rev. Lett. **18**, 1184 (1967).

[3]C. Zipfel and T. M. Sanders, Jr., in *Proceedings of the Eleventh International Conference on Low Temperature Physics,* edited by J. F. Allen, D. M. Finlayson, and D. M. McCall (University of St. Andrews, Scotland, 1968), Vol. I. p. 296.

[4]C. L. Zipfel, Ph.D. thesis, University of Michigan, 1969 (unpublished).

[5]T. Miyakawa and D. L. Dexter, Phys. Rev. A **1**, 513 (1970).

[6]C. C. Grimes and G. Adams, Phys. Rev. B **41**, 6366 (1990). Reexamination of the wavelength calibration and the corrections for lag and lash revealed that the photocurrent transition energies reported in this reference should be reduced by $\approx 1\%$. The corrected values are displayed in Fig. 3.

[7]A. Ya. Parshin and S. V. Pereverzev, Pis'ma Zh. Eksp. Teor. Fiz. **52**, 905 (1990) [JETP Lett. **52**, 282 (1990)].

[8]B. E. Springett, Phys. Rev. **155**, 139 (1967).

[9]L. D. Landau and E. M. Lifshitz, *Quantum Mechanics,* Vol. 3 of *Course of Theoretical Physics,* translated from the Russian by J. B. Sykes and J. S. Bell, 3rd ed. (Pergamon, Oxford, 1977), p. 110; E. Merzbacher, *Quantum Mechanics,* 2nd ed. (Wiley, New York, 1970), p. 198.

[10]M. Iino, M. Suzuki, and A. J. Ikushima, J. Low Temp. Phys. **61**, 155 (1985).

[11]R. F. Harris-Lowe and K. A. Smee, Phys. Rev. A **2**, 158 (1970).

[12]M. A. Woolf and G. W. Rayfield, Phys. Rev. Lett. **15**, 235 (1965).

[13]D. Amit and E. P. Gross, Phys. Rev. **145**, 130 (1966).

[14]E. P. Gross and H. Tung-Li, Phys. Rev. **170**, 190 (1968).

[15]Lord Rayleigh, *Theory of Sound* (Dover, New York, 1945), Vol. II, p. 372.

[16]R. J. Donnelly and P. H. Roberts, Proc. R. Soc. London, Ser. A **312**, 519 (1969).

[17]A. L. Fetter, Phys. Rev. **138**, 429 (1963).

[18]P. E. Parks and R. J. Donnelly, Phys. Rev. Lett. **16**, 45 (1966).
[19]B. DuVall and V. Celli, Phys. Rev. **180**, 276 (1969).
[20]W. B. Fowler and D. L. Dexter, Phys. Rev. **176**, 337 (1968).
[21]C. C. Klick and J. H. Schulman, in *Solid State Physics,* edited by F. Seitz and D. Turnbull (Academic, New York, 1957), Vol. 5.
[22]V. Celli, M. H. Cohen, and M. J. Zuckerman, Phys. Rev. **173**, 253 (1968).
[23]W. D. Johnson and D. G. Onn, J. Phys. C **11**, 3631 (1978).
[24]T. Miyakawa and D. L. Dexter, Phys. Rev. **184**, 166 (1969).
[25]A. J. Dahm, in *Progress in Low Temperature Physics,* edited by D. F. Brewer (North-Holland, Amsterdam, 1986), Vol. 10, p. 73.